Table I. Tumor response in 16 patients treated with cisplatin-based neoadjuvant chemotherapy.

	No. of patients					
	CR	PR	SD	PD	Response rate (%)	P-value
Total	0	4	12	0	25	
No. of tumors						0.569
Solitary	0	3	5	0	37.5	
Multiple	0	1	7	0	12.5	
Tumor size (cm)						>0.999
≤3	0	2	6	0	25	
>3	0	2	6	0	25	
Stage						0.435
I	0	3	4	0	43	
II	0	1	6	0	14	
III	0	0	2	0	0	

CR, complete response; PR, partial response; SD, stable disease; PD, progressive disease.

with 10% normal rabbit serum, and were then incubated overnight at 4°C with mouse anti-MRP2 monoclonal antibody (clone M2III-6; Monosan, Uden, The Netherlands; dilution at 1:20). Sections were then incubated with biotinylated rabbit anti-mouse immunoglobulin for 30 min followed by incubation with the streptavidin-peroxidase complex for 10 min. Diaminobenzidine was used as the chromogen, and the sections were counterstained with hematoxylin. Normal mouse immunoglobulin was substituted for the primary antibody as a negative control, whereas the immunoreactivity of adjacent non-neoplastic liver tissue was used as an internal positive control.

Pattern of MRP2 immunohistochemical expression in HCC. MRP2 expression was defined as the immunoreactivity of canalicular (apical) membranes of hepatocytes according to the description of Paulusma *et al* (4). Non-neoplastic hepatocytes showed weak to moderate intensity of MRP2 expression in the canalicular membrane. Immunoreactivity of MRP2 in tumor specimens was evaluated by comparison with adjacent non-neoplastic hepatocytes and classified into 3 categories: unchanged expression, when immunoreactivity of the tumor specimen was similar to that of non-neoplastic hepatocytes; loss-of-expression, characterized by totally negative immunoreactivity throughout the tumor specimen; and diffuse expression, characterized by strong positive immunoreactivity throughout the tumor specimen (Fig. 1). In the current study, overexpression of MRP2 was defined as diffuse expression, whereas non-overexpression was defined as unchanged or loss-of-expression.

Detection of MRP2 expression by Western blot analysis. Tissue samples were prepared for Western blotting by first snap-freezing and then stored at -80°C until used for analysis. Tissue samples from 3 normal livers obtained at surgery for other conditions were processed for analysis as normal controls. Lysate from tissue samples were obtained by homogenization in the lysis buffer [20 mM Tris-buffered with 4-(2-hydroxyethyl)-1-piperazineethanesulfonic acid (HEPES) pH 8.0, 2 mM ethylenediaminetetraacetic acid (EDTA), 0.5 M sodium chloride, 0.5% sodium deoxycholate, 0.5% Triton X-100, 0.25 M sucrose, 50 mM 2-mercapto-ethanol, 250 μM phenylmethylsulfonyl fluoride and 1 μM pepstatin]. The lysate samples were kept on ice for 30 min, filtered through gauze and precleared by centrifugation at 15,000 rpm for 15 min at 4°C. Following protein quantification using the Bradford assay (Bio-Rad Laboratories, Hercules, CA, USA), 50 μg aliquots of samples were resolved by sodium dodecyl sulfate-polyacrylamide gel electrophoresis and transferred to Immobilon membranes (Millipore, Bedford, MA, USA). Nonspecific sites binding sites on the membranes were blocked in 5% skim milk, whereupon filters were incubated with anti-MRP2 antibody (clone M2III-6; Monosan, Uden; dilution at 1:1000) and then the appropriate horseradish peroxidase-conjugated secondary antibodies. After the detection was performed using enhanced chemiluminescence reagent (GE Healthcare, Buckingham, UK), the blots were stripped, washed, and reprobed for ß-actin (Santa Cruz Biotechnology, Santa Cruz, CA, USA; dilution at 1:5000).

Statistical analysis. Medical records were obtained from all 49 patients. Categorical variables were compared by the Fisher exact test or the Pearson χ^2 test; continuous variables were compared by the Mann-Whitney U test. Correlation between 2 continuous variables was evaluated by the Spearman rank correlation. All statistical evaluations were performed using the SPSS 16.0J software package (SPSS Japan, Tokyo, Japan). All tests were two-sided and $P<0.05$ was considered statistically significant.

Results

Tumor response in 16 patients treated with cisplatin-based neoadjuvant chemotherapy. In 16 patients who received

Table II. Toxicity in 16 patients treated with cisplatin-based neoadjuvant chemotherapy.

Characteristics	No. of patients			
	Grade 1	Grade 2	Grade 3	Grade 4
Hematological toxicity				
Leukocytopenia	2	1	0	0
Anemia	0	1	0	0
Thrombocytopenia	2	2	0	0
Non-hematological toxicity				
Fever	2	0	0	0
Diarrhea	1	0	0	0
Decreased albumin level	2	7	0	0
Elevated total bilirubin level	4	1	0	0
Elevated AST level	2	8	2	0
Elevated ALT level	3	7	1	0
Elevated creatinine level	6	0	0	0

AST, aspartate aminotransferase; ALT, alanine aminotransferase.

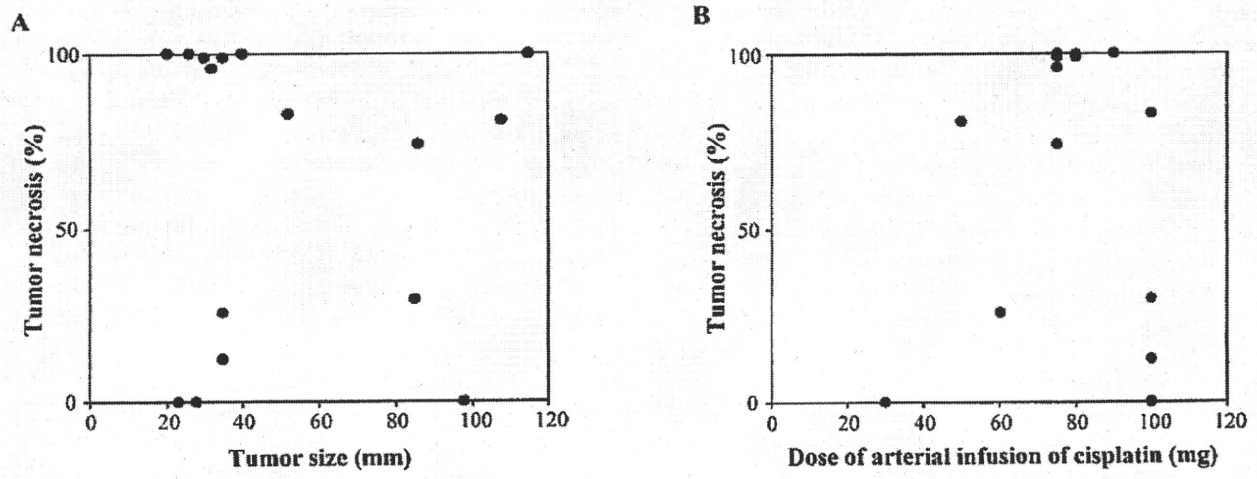

Figure 2. Correlation of tumor necrosis with tumor size and dose of cisplatin. (A) Tumor size prior to neoadjuvant chemotherapy does not correlate with tumor necrosis (correlation coefficient = -0.102; P=0.706). (B) The dose of hepatic arterial infusion of cisplatin has no correlation with tumor necrosis (correlation coefficient = -0.160; P=0.555).

cisplatin-based neoadjuvant chemotherapy, the median dose of cisplatin was 77.5 mg per body (range: 30-100 mg per body). The overall response rate of these patients was 25%; the therapeutic efficacy according to the RECIST guidelines was not associated with tested tumor-related factors (Table I).

Toxicity in 16 patients treated with cisplatin-based neoadjuvant chemotherapy. All 16 patients were assessed for toxicity and no toxic deaths occurred. The incidences of the main treatment-related toxicity according to the CTCAE version 4.0 are listed in Table II as the maximum grade seen per patient. No patients with grade 4 toxicities were identified. Three grade 3 non-hematological toxicities were observed. All hematological toxicities were grade 2.

Surgical resection. Hepatectomy procedures that were planned before neoadjuvant chemotherapy was administered were performed in all 16 patients who received the neoadjuvant chemotherapy. The interval between neoadjuvant chemotherapy and delayed surgery ranged from 30 to 114 days (median: 53 days). Operative procedures included major hepatectomy in 13 patients and minor hepatectomy in 36 patients. Complications during the postresection hospital stay occurred in 10 (20%) patients. Intra-abdominal sepsis (n=5) was the most common complication, followed by wound infection (n=4), biliary fistula (n=2), and pneumonia (n=1). The incidence of postoperative morbidity was 13% (2 of 16 patients) in patients treated with neoadjuvant chemotherapy compared with 24% (8 of 33 patients) in patients treated

Table III. Factors associated with MRP2 expression in 46 tumor specimens.

Variable	No. of patients		P-value
	Non-overexpression of MRP2	Overexpression of MRP2	
Age			0.568
≤70	13	12	
>70	9	12	
Sex			>0.999
Male	18	20	
Female	4	4	
Neoadjuvant chemotherapy			0.521
Absent	17	16	
Present	5	8	
Liver cirrhosis			0.763
Absent	7	9	
Present	15	15	
Tumor size (cm)			0.388
≤3	14	12	
>3	8	12	
Number of hepatic tumors			0.080
Solitary	16	11	
Multiple	6	13	
Edmondson-Steiner grade			0.507
I	4	4	
II	17	16	
III	1	4	
pT classification			0.625
pT1	13	11	
pT2	8	10	
pT3	1	3	
Vascular invasion			>0.999
Absent	18	20	
Present	4	4	

MRP2, multidrug resistance-associated protein 2; pT, pathologic T classification.

without neoadjuvant chemotherapy (P=0.464). There were no in-hospital deaths in the current series.

Tumor necrosis in resected specimens of 16 patients treated with cisplatin. The median percentage of histologically verified tumor necrosis was 81% (range: 0-100%). Complete tumor necrosis (no evidence of vivid tumor) was found in 3 patients [1 patient with PR (partial response) and 2 patients with SD (stable disease)], whereas no evidence of tumor necrosis was observed in 3 patients. Tumor size on CT images prior to neoadjuvant chemotherapy did not correlate with tumor necrosis of the resected specimens (P=0.706; Fig. 2A). The dose of hepatic arterial infusion of cisplatin did not correlate with tumor necrosis of the resected specimens (P=0.555; Fig. 2B). The median percentage of tumor necrosis was 99.4% (range: 73.6-100%) in 4 patients with PR, whereas it was 54.9% (range: 0-100%) in 12 patients with SD. There were no apparent differences in the percentage of tumor necrosis between 2 groups (PR vs. SD) according to the RECIST criteria by Mann-Whitney U test (P=0.138).

Immunohistochemical analysis of MRP2 expression. Three tissue samples with complete tumor necrosis were excluded from immunohistochemical analysis for MRP2. In the remaining 46 tissue samples, overexpression of MRP2 was detected in 24/46 (52%) of tumor specimens (Table III).

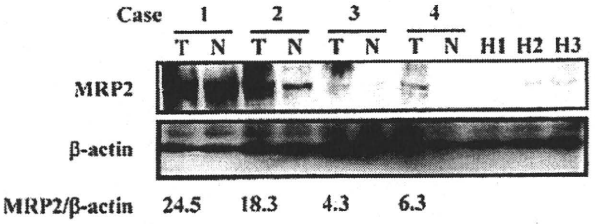

Figure 3. Western blot analysis for multidrug resistance-associated protein 2 (MRP2) levels. Based on immunohistochemical analysis, case 1 and 2 show overexpression of MRP2, whereas case 3 and 4 show non-overexpression of MRP2. The band intensities of tumor samples tested by Western blot analysis show a close correlation with the results of immunohistochemical analysis. MRP2 expression is faint in all healthy liver tissues. T; tumor, N; non-tumor, H1-3; healthy liver.

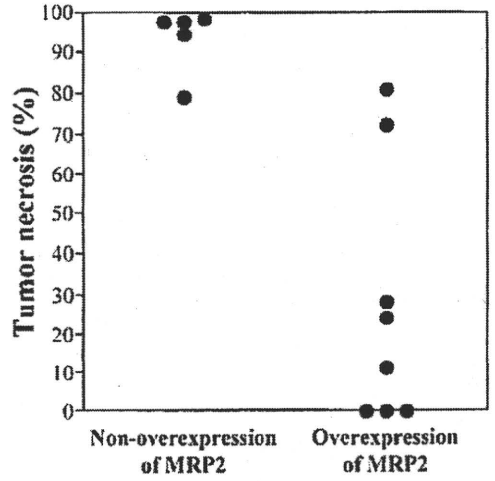

Figure 4. The extent of tumor necrosis in relation to the level of multidrug resistance-associated protein 2 (MRP2) expression. The percentage of tumor necrosis is significantly lower in tumor specimens with overexpression of MRP2 (median percentage of necrosis, 19%) than in tumor specimens with non-overexpression of MRP2 (median percentage of necrosis, 99%; P=0.003).

Loss-of-expression of MRP2 was found in 2/46 (4%) of tumor specimens; unchanged expression of MRP2 was observed in 20/46 (44%) of tumor specimens; and thus 22 tumor specimens were categorized as specimens with non-overexpression of MRP2.

Western blot analyses of MRP2 expression levels. To confirm the results of the immunohistochemical analysis for MRP2, we performed Western blot analysis on 5 randomly selected tumor samples with overexpression of MRP2, 5 tumor samples with non-overexpression of MRP2, and 3 tissue samples from healthy liver. Fig. 3 shows the representative results of Western blotting for MRP2 of selected tissue samples. MRP2 expression was faint in all healthy liver tissues tested by Western blot analysis, whereas the band intensities of tumor samples showed a close correlation with the results of immunohistochemical analysis.

Factors associated with MRP2 expression in 46 tumor specimens. Overexpression of MRP2 in tumor specimens was not associated with tested clinical-pathologic factors including neoadjuvant chemotherapy (Table III). Overexpression of MRP2 was detected in 16/33 (48%) of tumor specimens from patients treated without neoadjuvant chemotherapy, suggesting that nearly half of the patients with HCC have intrinsic overexpression of MRP2.

MRP2 expression and tumor necrosis in 13 tumor specimens containing vivid tumor from patients treated with cisplatin. We identified 8 tumor specimens with overexpression of MRP2 out of 13 tumor specimens containing vivid tumor from 16 patients treated with cisplatin-based neoadjuvant chemotherapy (Table III). Tumor specimens with overexpression of MRP2 showed a lower percentage of tumor necrosis (median percentage of necrosis, 19%) compared to tumor specimens with non-overexpression of MRP2 (median percentage of necrosis, 99%; P=0.003; Fig. 4).

Discussion

The activity of ABC transporters is one of the major causes of resistance to chemotherapy in patients with HCC (23). Of several identified ABC transporters, MRP2 is the principal cisplatin transporter (7-9). There is a paucity of clinical data regarding any relationship between MRP2 expression and tumor necrosis in patients treated with cisplatin-based neoadjuvant chemotherapy prior to hepatectomy for HCC. This prompted us to conduct the current study. This is the first study to demonstrate that MRP2 overexpression correlates with a lower percentage of tumor necrosis in tumors from patients treated with cisplatin-based neoadjuvant chemotherapy for HCC and thus expression of MRP2 determines the efficacy of cisplatin-based chemotherapy in patients with HCC.

Cisplatin is a widely used chemotherapeutic agent in the treatment of HCC (24). The fine-powder formulation of cisplatin has 3 times higher concentration compared to conventional formulations of cisplatin (25). Yoshikawa *et al* (25) reported that hepatic arterial infusion of a fine-powder formulation of cisplatin had a high therapeutic efficacy with a response rate of 33.8%. In the current study, we confirmed the results of Yoshikawa *et al* (25). Severe adverse effects (grade 3, liver dysfunction) were observed in 3 patients but they were manageable and transient. Planned hepatectomy procedures were performed in all 16 patients treated with neoadjuvant chemotherapy without any increase in post-operative complications. Thus, neoadjuvant chemotherapy with a fine-powder formulation of cisplatin is well tolerated and does not impair planned hepatectomy procedures.

We observed high tumor necrosis in the tumor specimens of patients who were treated with cisplatin-based neoadjuvant chemotherapy for HCC. In contrast, there were no apparent differences in the percentage of tumor necrosis between patients with PR and patients with SD according to RECIST criteria. In fact, complete tumor necrosis (no evidence of vivid tumor) was found in 2 patients with SD. Forner *et al* (26) have the questioned the reliability of RECIST criteria, which are based on the evaluation of unidimensional tumor measurements and disregard the extent of necrosis in solid liver tumors. Forner *et al* (26) recommended the evaluation

of tumor response based on measurements of the reduction in viable tumor burden as determined by dynamic imaging studies. Michaelis and Ratain (27) also suggested that RECIST criteria have limited value in the assessment of tumor response after chemotherapy because some anti-cancer agents have cytostatic, rather than cytotoxic properties, so that shrinkage of the tumor after cytostatic chemotherapy is not expected. Further investigation is required to develop effective criteria for the assessment of tumor response after chemotherapy.

MRP2 is a major transporter of conjugated bilirubin and bile salts into the bile canaliculi (5,6). In the current study, half of the tumor samples showed MRP2 overexpression, irrespective of administration of cisplatin (Table III). Since HCCs often produce bile, the intrinsic expression of MRP2 in HCC may partly explain their low sensitivity to some MRP2-dependent anti-cancer agents including cisplatin, doxorubicin, etoposide, and vincristine (7,28). Bonin *et al* documented that MRP2 mRNA expression level significantly increases in HCC compared to non-neoplastic liver tissue (14). In addition, Zollner *et al* using Western blot analysis found that MRP2 protein expression was elevated in all 4 HCC samples examined (13). In the current study, overexpression of MRP2 correlated with a lower percentage of tumor necrosis in patients treated with cisplatin-based neoadjuvant chemotherapy for HCC, whereas tumor size or dose of cisplatin did not. Collectively, these above findings suggest that expression of MRP2 determines the efficacy of cisplatin-based chemotherapy in patients with HCC.

Various classic compounds that inhibit MRP2 activity *in vitro* such as MK-571 or cyclosporin A have been proposed to be used to increase antitumor therapeutic effectiveness (29,30). The intrinsic toxicity of MRP2 inhibitors at doses necessary for their activity and their poor specificity are the major obstacles in applying them *in vivo* (8). In attempt to develop alternative, less toxic, and more efficient therapy, Meterna *et al* specifically inhibited MRP2 protein expression by 2 anti-MRP2 hammerhead ribozymes. This gene therapeutic approach may be applicable to overcome cisplatin resistance in tumor cells (8). Folmer *et al* demonstrated that tumors resulting from MRP2-overexpressing subcutaneously grown hepatoma cells, regressed in size upon antisense MRP2 expression in combination with vincristine (28). Wakamatsu *et al* reported that co-treatment with cisplatin and both glycyrrhizin and lamivudine inhibited the cisplatin efflux from Huh7 HCC cell line and concluded this was because glycyrrhizin is a competitive substrate for MRP2 (9). Therefore, it appears that inhibition of MRP2 may be an approach to develop an effective therapy to overcome cisplatin resistance in patients with HCC.

In interpreting the current study, we have considered the limitations of the analysis of a small number of patients and incomplete follow-up assessment of performed chemotherapeutic treatment using RECIST criteria. In fact, we believe that these limitations do not greatly influence the results of the study because the differences among groups were too marked to have resulted from these procedural biases.

In conclusion, overexpression of MRP2 correlates with a lower percentage of tumor necrosis in patients treated with cisplatin-based neoadjuvant chemotherapy for HCC, whereas either tumor size or dose of cisplatin does not. Expression of MRP2 determines the efficacy of cisplatin-based chemotherapy in patients with HCC.

References

1. Dean M, Rzhetsky A and Allikmets R: The human ATP-binding cassette (ABC) transporter superfamily. Genome Res 11: 1156-1166, 2001.
2. Mayer R, Kartenbeck J, Büchler M, Jedlitschky G, Leier I and Keppler D: Expression of the MRP gene-encoded conjugate export pump in liver and its selective absence from the canalicular membrane in transport-deficient mutant hepatocytes. J Cell Biol 131: 137-150, 1995.
3. Keppler D and Kartenbeck J: The canalicular conjugate export pump encoded by the *cmrp/cmoat* gene. In: Progress in Liver Diseases. Boyer JL and Ockner RK (eds). Saunders, Philadelphia, PA, pp55-67, 1996.
4. Paulusma CC, Kool M, Bosma PJ, Scheffer GL, ter Borg F, Scheper RJ, Tytgat GN, Borst P, Baas F and Oude Elferink RP: A mutation in the human canalicular multispecific organic anion transporter gene causes the Dubin-Johnson syndrome. Hepatology 25: 1539-1542, 1997.
5. Jedlitschky G, Leier I, Buchholz U, Hummel-Eisenbeiss J, Burchell B and Keppler D: ATP-dependent transport of bilirubin glucuronides by the multidrug resistance protein MRP1 and its hepatocyte canalicular isoform MRP2. Biochem J 327: 305-310, 1997.
6. Trauner M and Boyer JL: Bile salt transporters: molecular characterization, function, and regulation. Physiol Rev 83: 633-671, 2003.
7. Cui Y, König J, Buchholz JK, Spring H, Leier I and Keppler D: Drug resistance and ATP-dependent conjugate transport mediated by the apical multidrug resistance protein, MRP2, permanently expressed in human and canine cells. Mol Pharmacol 55: 929-937, 1999.
8. Materna V, Liedert B, Thomale J and Lage H: Protection of platinum-DNA adduct formation and reversal of cisplatin resistance by anti-MRP2 hammerhead ribozymes in human cancer cells. Int J Cancer 115: 393-402, 2005.
9. Wakamatsu T, Nakahashi Y, Hachimine D, Seki T and Okazaki K: The combination of glycyrrhizin and lamivudine can reverse the cisplatin resistance in hepatocellular carcinoma cells through inhibition of multidrug resistance-associated proteins. Int J Oncol 31: 1465-1472, 2007.
10. Koike K, Kawabe T, Tanaka T, Toh S, Uchiumi T, Wada M, Akiyama S, Ono M and Kuwano M: A canalicular multispecific organic anion transporter (cMOAT) antisense cDNA enhances drug sensitivity in human hepatic cancer cells. Cancer Res 57: 5475-5479, 1997.
11. Nies AT, König J, Pfannschmidt M, Klar E, Hofmann WJ and Keppler D: Expression of the multidrug resistance proteins MRP2 and MRP3 in human hepatocellular carcinoma. Int J Cancer 94: 492-499, 2001.
12. Vander Borght S, Libbrecht L, Blokzijl H, Faber KN, Moshage H, Aerts R, Van Steenbergen W, Jansen PL, Desmet VJ and Roskams TA: Diagnostic and pathogenetic implications of the expression of hepatic transporters in focal lesions occurring in normal liver. J Pathol 207: 471-482, 2005.
13. Zollner G, Wagner M, Fickert P, Silbert D, Fuchsbichler A, Zatloukal K, Denk H and Trauner M: Hepatobiliary transporter expression in human hepatocellular carcinoma. Liver Int 25: 367-379, 2005.
14. Bonin S, Pascolo L, Crocé LS, Stanta G and Tiribelli C: Gene expression of ABC proteins in hepatocellular carcinoma, perineoplastic tissue, and liver diseases. Mol Med 8: 318-325, 2002.
15. Cruz PV, Wakai T, Shirai Y, Yokoyama N and Hatakeyama K: Loss of carcinoembryonic antigen-related cell adhesion molecule 1 expression is an adverse prognostic factor in hepatocellular carcinoma. Cancer 104: 354-360, 2005.
16. Wakai T, Shirai Y, Sakata J, Kaneko K, Cruz PV, Akazawa K and Hatakeyama K: Anatomic resection independently improves long-term survival in patients with T1-T2 hepatocellular carcinoma. Ann Surg Oncol 14: 1356-1365, 2007.
17. Korita PV, Wakai T, Shirai Y, Matsuda Y, Sakata J, Cui X, Ajioka Y and Hatakeyama K: Overexpression of osteopontin independently correlates with vascular invasion and poor prognosis in patients with hepatocellular carcinoma. Hum Pathol 39: 1777-1783, 2008.

18. Therasse P, Arbuck SG, Eisenhauer EA, Wanders J, Kaplan RS, Rubinstein L, Verweij J, Van Glabbeke M, van Oosterom AT, Christian MC and Gwyther SG: New guidelines to evaluate the response to treatment in solid tumors. European Organization for Research and Treatment of Cancer, National Cancer Institute of the United States, National Cancer Institute of Canada. J Natl Cancer Inst 92: 205-216, 2000.
19. Cancer Therapy Evaluation Program. Common Terminology Criteria for Adverse Events. Version 4.0. National Cancer Institute. Available from URL: http://ctep.cancer.gov/protocolDevelopment/electronic_applications/ctc.htm.
20. Sobin LH and Wittekind C: TNM Classification of Malignant Tumours. 6th edition. UICC, Wiley-Liss, New York, pp81-83, 2002.
21. Taylor M, Forster J, Langer B, Taylor BR, Greig PD and Mahut C: A study of prognostic factors for hepatic resection for colorectal metastases. Am J Surg 73: 467-471, 1997.
22. Edmondson HA and Steiner PE: Primary carcinoma of the liver: a study of 100 cases among 48,900 necropsies. Cancer 7: 462-503, 1954.
23. Le Vee M, Jigorel E, Glaise D, Gripon P, Guguen-Guillouzo C and Fardel O: Functional expression of sinusoidal and canalicular hepatic drug transporters in the differentiated human hepatoma HepaRG cell line. Eur J Pharm Sci 28: 109-117, 2006.
24. Carr BI: Hepatocellular carcinoma: current management and future trends. Gastroenterology 127 (Suppl 1): S218-S224, 2004.
25. Yoshikawa M, Ono N, Yodono H, Ichida T and Nakamura H: Phase II study of hepatic arterial infusion of a fine-powder formulation of cisplatin for advanced hepatocellular carcinoma. Hepatol Res 38: 474-483, 2008.
26. Forner A, Ayuso C, Varela M, Rimola J, Hessheimer AJ, de Lope CR, Reig M, Bianchi L, Llovet JM and Bruix J: Evaluation of tumor response after locoregional therapies in hepatocellular carcinoma: are response evaluation criteria in solid tumors reliable? Cancer 115: 616-623, 2009.
27. Michaelis LC and Ratain MJ: Measuring response in a post-RECIST world: from black and white to shades of grey. Nat Rev Cancer 6: 409-414, 2006.
28. Folmer Y, Schneider M, Blum HE and Hafkemeyer P: Reversal of drug resistance of hepatocellular carcinoma cells by adenoviral delivery of anti-ABCC2 antisense constructs. Cancer Gene Ther 14: 875-884, 2007.
29. Leier I, Jedlitschky G, Buchholz U, Cole SP, Deeley RG and Keppler D: The MRP gene encodes an ATP-dependent export pump for leukotriene C4 and structurally related conjugates. J Biol Chem 269: 27807-27810, 1994.
30. Chen ZS, Kawabe T, Ono M, Aoki S, Sumizawa T, Furukawa T, Uchiumi T, Wada M, Kuwano M and Akiyama SI: Effect of multidrug resistance-reversing agents on transporting activity of human canalicular multispecific organic anion transporter. Mol Pharmacol 56: 1219-1228, 1999.

Dig Dis Sci (2010) 55:3576–3583
DOI 10.1007/s10620-010-1222-5

ORIGINAL ARTICLE

Clinical Advantage of Highly Sensitive On-Chip Immunoassay for Fucosylated Fraction of Alpha-Fetoprotein in Patients with Hepatocellular Carcinoma

Yasushi Tamura · Masato Igarashi · Hirokazu Kawai · Takeshi Suda · Shinji Satomura · Yutaka Aoyagi

Received: 16 January 2010 / Accepted: 23 March 2010 / Published online: 21 April 2010

Abstract
Background Alpha-fetoprotein (AFP) has been widely used as a diagnostic master for hepatocellular carcinoma (HCC), and the fucosylated fraction of AFP (AFP-L3) has been reported to be a specific marker for HCC. However, AFP-L3 has not always been reliable in cases with low serum AFP concentrations. Recently, a novel automated immunoassay for AFP-L3, the micro-total analysis system (μ-TAS), has been developed.
Aim The aim of this study is to evaluate the clinical usefulness of μ-TAS AFP-L3.
Methods Serum AFP-L3 was measured in 295 patients with HCC and in 350 with benign liver diseases. The diagnostic accuracy of μ-TAS AFP-L3 was compared with that of the conventional assay (liquid-phase binding assay; LiBASys). The relationship between μ-TAS AFP-L3 and clinical features was investigated.
Results When the cutoff value was set at 7%, the sensitivity, specificity, accuracy, positive predictive value, and negative predictive value of μ-TAS AFP-L3 were 60.0%, 90.3%, 76.4%, 83.9%, and 72.8%, respectively. Its sensitivity was particularly good (41.1%) in HCC subgroups with lower AFP concentrations (<20 ng/ml). The positivity rates for μ-TAS AFP-L3 were higher at each tumor stage than those of LiBASys AFP-L3 (μ-TAS/LiBASys: stage I, 44.2%/16.3%; stage II, 52.9%/37.5%; stage III, 66.4%/44.5%; stage IV, 82.8%/65.5%).
Conclusions μ-TAS AFP-L3 is more sensitive for discriminating HCC than the conventional LiBASys AFP-L3, particularly in subgroups with lower AFP concentrations and early-stage HCC.

Keywords Alpha-fetoprotein · AFP-L3 · Diagnosis · Hepatocellular carcinoma

Introduction

Alpha-fetoprotein (AFP) has been widely used as a diagnostic marker for hepatocellular carcinoma (HCC) [1, 2]. However, AFP levels are sometimes elevated in patients with chronic hepatitis and cirrhosis who have no evidence of HCC [3–5]. Therefore, the usefulness of AFP as a screening marker of HCC has been limited by its impaired specificity.

The fucosylated fraction of AFP (AFP-L3) has been reported to be a specific marker for HCC [6–8]. Moreover, its level predicts the malignant potential of HCC with subsequent unfavorable prognosis after treatment [9–13]. However, measurement of AFP-L3 has not always been reliable for serum samples with low total AFP concentration determined by conventional lectin affinity electrophoresis or using a liquid-phase binding assay system (LiBASys) [14].

Recently, a novel automated immunoassay for AFP-L3 using on-chip electrokinetic reaction and separation by affinity electrophoresis (micro-total analysis system; μ-TAS) has been developed [15, 16]. This system involves microchip capillary electrophoresis and a liquid-phase

Y. Tamura (✉) · M. Igarashi · H. Kawai · T. Suda · Y. Aoyagi
Division of Gastroenterology and Hepatology, Niigata University Graduate School of Medical and Dental Sciences, 757 Asahimachi Dori-1-Bancho, Chuo-ku, Niigata 951-8520, Japan
e-mail: ytamura@med.niigata-u.ac.jp

S. Satomura
Diagnostic Division, Wako Pure Chemical Industries Ltd., Osaka, Japan

binding assay system, and the assay can be run in less than 10 min.

The aim of this study is to evaluate the clinical usefulness of measuring μ-TAS AFP-L3 as a diagnostic and prognostic marker in comparison with the conventional LiBASys AFP-L3 assay.

Methods

Patients

Frozen serum samples were obtained from 295 patients with HCC and from 350 patients with benign liver diseases (BLD) who had chronic hepatitis or liver cirrhosis between April 1999 and September 2009. Among the BLD patients, 80 were positive for hepatitis B surface antigen (HBsAg), 167 were positive for anti-hepatitis C virus (HCV), 19 had autoimmune hepatitis, 51 had primary biliary cirrhosis, 17 had alcoholic liver disease, 11 had nonalcoholic steatohepatitis, and 5 had other conditions. HCC patients were diagnosed using imaging modalities such as computed tomography (CT), magnetic resonance imaging (MRI), and CT during hepatic arteriography, considering hyperattenuation in the arterial phase with washout in the late phase. Vascular invasion was evaluated by imaging modalities. In some cases that showed atypical features on imaging, ultrasound-guided biopsies were performed. Tumor stage on imaging findings was ranked using the tumor–node–metastasis (TNM) staging system of the Liver Cancer Study Group of Japan [17, 18]: T1 (fulfilling the following three conditions: solitary, ≤2 cm, no vessel invasion), T2 (fulfilling two of the three conditions), T3 (fulfilling one of the three conditions), T4 (fulfilling none of the three conditions or showing presence of distant metastasis), N0 (no lymph nodes metastasis), N1 (metastasis to lymph nodes), M0 (no distant metastasis), M1 (distant metastasis), and stage I (T1N0M0), stage II (T2N0M0), stage III (T3N0M0), and stage IV (T4N0M0, or any TN1M0, or any TN0-1M1).

Therapeutic modalities for HCC patients were chosen on the basis of hepatic functional reserve, tumor multiplicity, and tumor size. Among the 295 HCC patients, 94 underwent hepatic resection, 60 underwent radiofrequency ablation (RFA) or microwave coagulation therapy (MCT), 32 underwent percutaneous ethanol injection (PEI), 48 underwent transcatheter arterial chemoembolization (TACE), 40 underwent transcatheter arterial infusion chemotherapy (TAI), 10 underwent systemic chemotherapy, and 11 received best supportive care. Long-term survival data for these HCC patients were confirmed at the end of October 2009.

Informed consent was obtained from each patient, and the study protocol conformed with the ethical guidelines of the 1975 Declaration of Helsinki, as reflected in the a priori approval by our institution's human research committee.

Laboratory Examination

Simultaneous quantitative measurement of AFP-L1 (ng/ml) and AFP-L3 (ng/ml) was achieved using the μ-TAS assay (Wako Pure Chemical Industries Ltd., Osaka, Japan) [15, 16], and then the percentage of AFP-L3 was calculated. As a reference method, AFP-L1 and AFP-L3 were also measured using a liquid-phase binding assay system (LiBASys) at the same time (Wako Pure Chemical Industries Ltd., Osaka, Japan) [14]. Total AFP concentration (ng/ml) in the serum sample was determined by addition of AFP-L3 to AFP-L1. Serum des-gamma-carboxy prothrombin (DCP) was measured using a μ-TAS assay for DCP (Wako Pure Chemical Industries Ltd, Osaka, Japan). The lower limits of quantitation for μ-TAS assay AFP (L1 and L3), LiBASys assay AFP (L1 and L3), and μ-TAS assay DCP are 0.3 ng/ml AFP (L1 and L3), 0.8 ng/ml AFP (L1 and L3), and 5 mAU/ml DCP, respectively [14–16]. When AFP-L3 is not detectable, the percentage of AFP-L3 is defined as 0.5%. AFP, AFP-L3, and DCP were measured in the same serum before treatment of HCC. Hepatic functional reserve was ranked using the criteria of the Child–Pugh scoring system.

Statistical Analysis

The correlations of the μ-TAS assay with the LiBASys assay were evaluated using the Pearson product-moment correlation coefficient. Receiver operating characteristic (ROC) analysis was used to evaluate the diagnostic value of the μ-TAS AFP-L3 assay and the LiBASys assay. Sensitivity, specificity, accuracy, positive predictive value, and negative predictive value of the μ-TAS assay AFP, AFP-L3, DCP, and LiBASys assay AFP-L3 were calculated.

Long-term survival of patients with HCC was determined by Kaplan–Meier method. Log-rank test was used to test for equality of long-term survival between groups. Multivariate analyses of prognostic factors in the clinical features were performed using the Cox proportional-hazards model. The factors included in multivariate analysis were patient age, gender (female/male), HBsAg (negative/positive), anti-HCV (negative/positive), alcohol intake (not frequent/frequent), Child–Pugh class (A/B, C), log (AFP ng/mL), log (DCP mAU/mL), μ-TAS assay AFP-L3 (%) (<7/≥7), tumor size (mm), number of tumors (single/multiple), vascular invasion (negative/positive), and

treatment method (hepatic resection/RFA, PEI, TACE, TAI). Statistical analyses were performed by using the SPSS 15.0 software package (SPSS Japan Inc., Tokyo, Japan). Differences at $P < 0.05$ were considered to be statistically significant.

Results

Clinical Features of Patients

Demographics, etiology of liver disease, hepatic functional reserve ranked by Child–Pugh classification, and tumor stage of the study patients are summarized in Table 1. Two hundred ninety-five patients with HCC comprised 43 patients with stage I, 104 with stage II, 119 with stage III, and 29 with stage IV.

Serum total AFP concentration and AFP-L3% in the HCC group and the BLD group are shown in Table 2.

Table 1 Clinical features of patients with HCC and BLD

	HCC ($n = 295$)	BLD ($n = 350$)
Age, median (range), years	70 (38–89)	60 (16–86)
Gender (female/male)	95/200	196/154
Etiology		
HBsAg (+)	69	80
Anti-HCV (+)	172	167
AIH	4	19
PBC	3	51
Alcoholic	27	17
NASH	7	11
Others	13	5
Child–Pugh class		
A/B/C	193/85/13	246/22/12
Tumor stage		
I/II/III/IV	43/104/119/29	
Therapeutic modality		
Hepatic resection	94	
RFA or MCT	60	
PEI	32	
TACE	48	
TAI	40	
Systemic chemotherapy	10	
Best supportive care	11	

HCC hepatocellular carcinoma, *BLD* benign liver disease, *HBsAg* hepatitis B surface antigen, *HCV* hepatitis C virus, *AIH* autoimmune hepatitis, *PBC* primary biliary cirrhosis, *NASH* nonalcoholic steatohepatitis, *RFA* radiofrequency ablation, *PEI* percutaneous ethanol injection, *TACE* transcatheter arterial chemoembolization, *TAI* transcatheter arterial infusion chemotherapy

Table 2 Serum total AFP concentration and AFP-L3% in patients with HCC and BLD

	HCC ($n = 295$)	BLD ($n = 350$)
LiBASys assay		
AFP ng/ml, median (range)	43.2 (0.8–1054374.1)	1.2 (0.8–1,767)
AFP-L3%, median (range)	1.3 (0.5–94.5)	0.5 (0.5–16.5)
μ-TAS assay		
AFP ng/ml, median (range)	51.1 (1.1–921613.9)	2.8 (0.3–1648.8)
AFP-L3%, median (range)	9.2 (0.5–97.0)	0.5 (0.5–17.3)

HCC hepatocellular carcinoma, *BLD* benign liver disease, *AFP* alpha-fetoprotein, *AFP-L3* fucosylated fraction of AFP, *LiBASys* liquid-phase binding assay system, *μ-TAS* micro-total analysis system

Correlations of the μ-TAS Assay with the LiBASys Assay for Total AFP Concentration and AFP-L3%

The correlation of the μ-TAS assay with the LiBASys assay for total AFP was evaluated. A correlation coefficient of 0.997 and a slope of 0.926 indicated good correlation between the two methods in 586 patients whose serum total AFP concentration was less than 1,000 ng/ml (Fig. 1a). AFP-L3 was also evaluated, and this revealed that the serum AFP-L3 level determined by using the μ-TAS assay correlated well ($r = 0.965$) with that determined by the LiBASys assay (Fig. 1b). However, the correlation became weaker for serum in which AFP was less than 20 ng/ml ($r = 0.387$) (Fig. 1c).

Comparison of Diagnostic Efficacy Between μ-TAS AFP-L3 and LiBASys AFP-L3

ROC curves for serum AFP-L3 examined by using the μ-TAS assay and the LiBASys assay are shown in Fig. 2. The area under the curve of μ-TAS AFP-L3 (0.858) was larger than that of LiBASys AFP-L3 (0.744), indicating that the diagnostic accuracy of AFP-L3 examined using the μ-TAS assay was superior to that obtained using the LiBASys assay.

We compared the diagnostic efficacy between μ-TAS AFP-L3 and LiBASys AFP-L3 at several cutoff values. The sensitivity, specificity, accuracy, positive predictive value, and negative predictive value of μ-TAS AFP-L3, LiBASys AFP-L3, μ-TAS AFP (cutoff 200 ng/ml), and μ-TAS DCP (cutoff 40 mAU/ml) are shown in Table 3a.

A cutoff value of 1% yielded the maximum value of Youden index (specificity/100 + sensitivity/100 − 1) of 0.637, when examined using the μ-TAS AFP-L3 assay. A cutoff value of 10% has been used for diagnosis of HCC in previous reports [8, 10–13, 19]. Additionally, we have

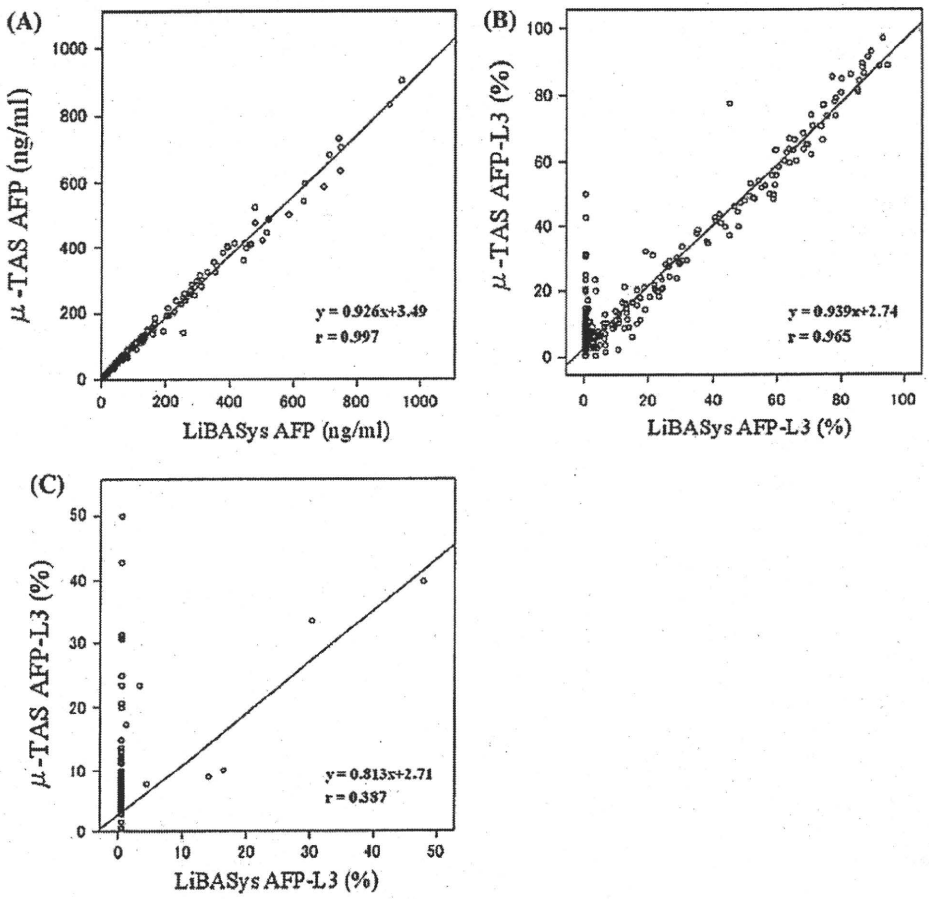

Fig. 1 Correlations of the μ-TAS assay with the LiBASys assay in terms of total AFP concentration (**a**), AFP-L3% (**b**), and AFP-L3% in subgroup with lower serum AFP concentration (<20 ng/ml) (**c**). Good correlation for AFP (correlation coefficient $r = 0.997$; slope 0.926) was observed between the μ-TAS assay and the LiBASys assay (**a**). The serum AFP-L3 level determined by the μ-TAS assay was well correlated ($r = 0.965$) with that determined by the LiBASys assay (**b**). The correlation became weaker for serum in which AFP was less than 20 ng/ml ($r = 0.387$) (**c**)

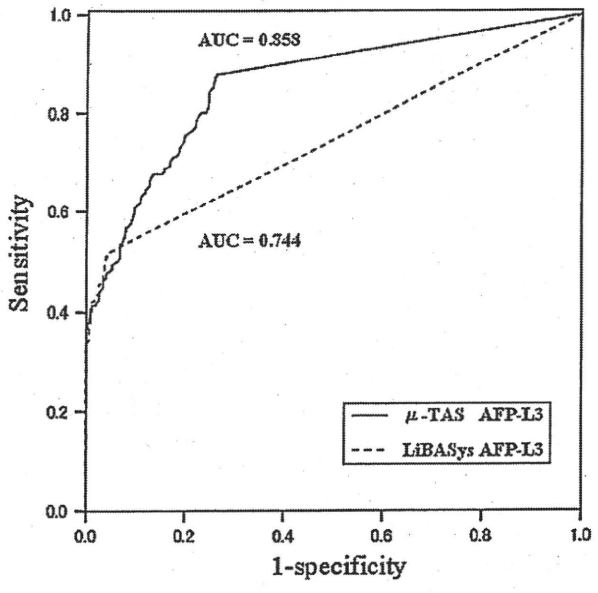

Fig. 2 Receiver operating characteristic curve for serum AFP-L3 examined using the μ-TAS and LiBASys assays. The area under the curve of μ-TAS AFP-L3 (0.858) was larger than that of LiBASys AFP-L3 (0.744)

chosen a cutoff value of 7%, which had been demonstrated to improve the sensitivity of the μ-TAS AFP-L3 assay greatly, and to maintain the specificity at 90% or more. The μ-TAS AFP-L3 was more sensitive for discriminating HCC than the LiBASys AFP-L3 at three cutoff levels with a small decrease of specificity compared with the LiBASys AFP-L3. In addition, μ-TAS AFP-L3 (cutoff 7%, 60.0%) was more sensitive for discriminating HCC than the total AFP level (cutoff 200 ng/ml, 33.6%) and μ-TAS DCP (cutoff 40 mAU/ml, 55.8%), which has been used as a standard marker for HCC. The diagnostic accuracies of μ-TAS AFP-L3 were superior to those of LiBASys AFP-L3 and μ-TAS AFP.

This diagnostic advantage of μ-TAS AFP-L3 was also observed in 432 patients (HCC, 112; BLD, 320) who had lower serum total AFP concentrations (less than 20 ng/ml). Serum AFP-L3% measured using the μ-TAS assay and the LiBASys assay in the lower serum AFP group is shown in Fig. 3a, b. The sensitivity, specificity, accuracy, positive predictive value, and negative predictive value of serum AFP-L3% calculated using three cutoff values (1%, 7%, and 10%) to determine HCC in the lower serum AFP group are shown in Table 3b. The sensitivity of μ-TAS AFP-L3 was especially good (μ-TAS/LiBASys: cutoff 1%,

Table 3 Sensitivity, specificity, accuracy, positive predictive values, and negative predictive values of μ-TAS AFP-L3, LiBASys AFP-L3, μ-TAS AFP, and μ-TAS DCP

	Cutoff	Sensitivity	Specificity	Accuracy	PPV	NPV
(A)						
LiBASys AFP-L3	1%	50.8%	95.7	75.2	90.9	69.8
	7%	40.0	99.1	72.1	97.5	66.2
	10%	38.3	99.4	71.5	98.3	65.7
μ-TAS AFP-L3	1%	87.5	73.7	80.0	73.7	87.5
	7%	60.0	90.3	76.4	83.9	72.8
	10%	47.5	96.0	73.8	90.9	68.4
μ-TAS AFP	200 ng/ml	33.6	98.0	68.5	93.4	63.6
μ-TAS DCP	40 mAU/ml	55.8	95.3	76.9	91.1	71.5
(B)						
LiBASys AFP-L3	1%	4.5	99.4	74.8	71.4	74.8
	7%	3.6	100	75.0	100	74.8
	10%	3.6	100	75.0	100	74.8
μ-TAS AFP-L3	1%	67.9	80.6	77.3	55.1	87.8
	7%	41.1	91.9	78.7	63.9	81.7
	10%	21.4	96.9	77.3	70.6	77.9

PPV positive predictive value, *NPV* negative predictive value, *AFP* alpha-fetoprotein, *AFP-L3* fucosylated fraction of AFP, *LiBASys* liquid-phase binding assay system, *μ-TAS* micro-total analysis system, *DCP* des-gamma-carboxy prothrombin

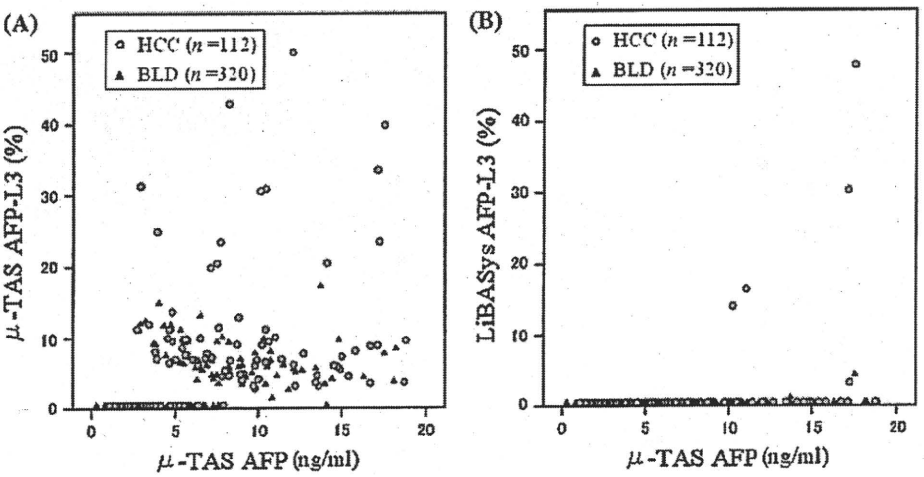

Fig. 3 Serum AFP-L3% measured using the μ-TAS and LiBASys assays in the lower serum AFP group (less than 20 ng/ml). μ-TAS assay (**a**) and LiBASys assay (**b**)

67.9%/4.5%; cutoff 7%, 41.1%/3.6%; cutoff 10%, 21.4%/3.6%) in the subgroups with lower AFP concentrations (<20 ng/ml). The diagnostic accuracy of μ-TAS AFP-L3 was superior to that of LiBASys AFP-L3, and the cutoff value of 7% for μ-TAS AFP-L3 had the most accurate diagnostic power (accuracy, 78.7%).

AFP-L3 Positivity Rate in Relation to Tumor Characteristics

When the cutoff value of AFP-L3 was set at 7%, the positivity rates for μ-TAS AFP-L3 were higher for each tumor stage (44.2% for stage I, 52.9% for stage II, 66.4% for stage III, 82.8% for stage IV) than those for LiBASys AFP-L3 (16.3% for stage I, 37.5% for stage II, 44.5% for stage III, 65.5% for stage IV). High positivity rates for μ-TAS AFP-L3 were also found in patients classified by tumor size and tumor number (μ-TAS/LiBASys: tumor size ≤2 cm, 43.5%/22.9%; 2 cm < tumor size ≤ 3 cm, 57.8%/37.1%; 3 cm < tumor size, 76.4%/57.5%; single tumor, 53.5%/32.7%; multiple tumors, 63.4%/43.8%) (Table 4).

Impact of μ-TAS AFP-L3 on Long-Term Survival of Patients with HCC

We evaluated the impact of μ-TAS AFP-L3 on the long-term survival of patients with HCC. The mean observation time after treatment was 23.5 months (range 0–106 months). The survival rate of patients with elevated μ-TAS

Table 4 Positivity rate of AFP-L3 at a 7% cutoff value according to tumor characteristics

	μ-TAS AFP-L3 (%)	LiBASys AFP-L3 (%)
Stage		
I	44.2	16.3
II	52.9	37.5
III	66.4	44.5
IV	82.8	65.5
Size (cm)		
≤2.0	43.5	22.9
2.1–3.0	57.8	37.1
3.0<	76.4	57.5
Number		
Single	53.5	32.7
Multiple	63.4	43.8

AFP-L3 fucosylated fraction of AFP, *μ-TAS* micro-total analysis system, *LiBASys* liquid-phase binding assay system

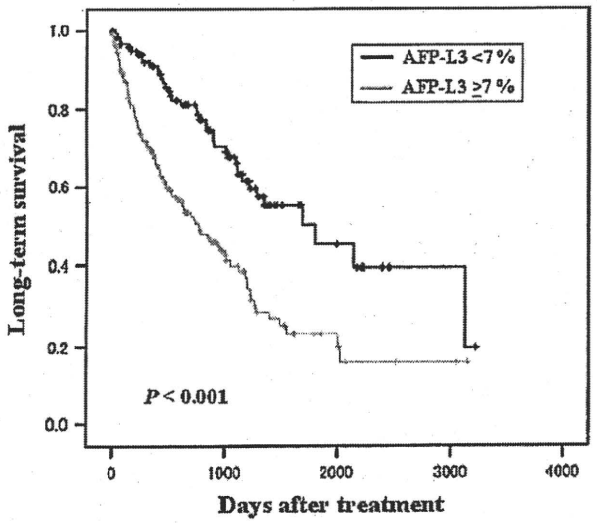

Fig. 4 Comparison of long-term survival rates between HCC patients with and without μ-TAS AFP-L3 elevation. *P* value was calculated using log-rank test

AFP-L3 level (≥7%) was significantly lower than that of patients without such elevation ($P < 0.001$) (Fig. 4).

Multivariate analysis using a Cox proportional-hazard model revealed that μ-TAS AFP-L3 status ($P = 0.021$) was a significant independent factor predictive of long-term survival in patients with HCC (Table 5). Child–Pugh class ($P < 0.001$), log (AFP ng/mL) ($P = 0.002$), number of tumors ($P = 0.001$), vascular invasion ($P = 0.010$), and treatment method ($P = 0.019$) were also significant independent prognostic factors.

Discussion

Many studies have shown that AFP-L3 status is a specific marker for HCC. However, measurement of AFP-L3 has not always been reliable in cases with low serum total AFP concentration. Furthermore, several studies have reported that the sensitivity of AFP-L3 is relatively low (22.2–38.0%) in early-stage HCCs less than 2 cm in diameter [8, 19].

In the present study we demonstrated that μ-TAS AFP-L3 was more sensitive and accurate for discriminating HCC from BLD than the conventional LiBASys AFP-L3 and total AFP level (cutoff 200 ng/ml), which have been used as a standard marker for HCC.

Diagnostic sensitivity was especially good in subgroups with lower AFP concentrations (<20 ng/ml). A cutoff level of 10% or 15% for AFP-L3 has been used for diagnosis of HCC in many previous studies [8, 10–13, 19]. In the present study, we compared the sensitivity, specificity, accuracy, positive predictive value, and negative predictive value for AFP-L3 between the μ-TAS assay and the conventional LiBASys assay at several cutoff values. We had suggested that a cutoff value of 7% was appropriate for discriminating HCC from BLD in the μ-TAS AFP-L3 assay. This cutoff value of 7% has been demonstrated to improve sensitivity greatly with a slight decrease of specificity as compared with the conventional LiBASys assay. The 7% cutoff value in the μ-TAS AFP-L3 had the highest diagnostic accuracy in the subgroups with lower AFP concentrations.

The difficulty in the treatment of HCC is related to the underlying impairment of hepatic functional reserve and late detection, thus limiting the possibility of curative therapy such as hepatic resection and RFA. Therefore, early detection of HCC followed by adequate curative treatment is an important issue for HCC surveillance in high-risk populations such as patients with cirrhosis due to any cause and chronic infection with hepatitis B virus or hepatitis C virus. From this viewpoint, μ-TAS AFP-L3 is an extremely powerful tool for detection of HCC at an early stage. The present study revealed that μ-TAS AFP-L3 (cutoff 7%) was able to detect HCC in 41.1% of patients with low AFP concentration (<20 ng/ml), compared with only 3.6% in the same subgroup using LiBASys AFP-L3. Theoretically, the μ-TAS AFP-L3% cutoff level could be measured for samples containing as little as 3 ng/ml total AFP [16]. Indeed, the μ-TAS AFP-L3 at a 7% cutoff value was able to detect 28 out of 80 (35.0%) HCC patients whose serum total AFP concentrations were less than 10 ng/ml. In contrast, AFP-L3% was not detected by the LiBASys assay at such low total AFP concentrations. In addition, the AFP-L3 positivity rate for the μ-TAS assay at

Table 5 Multivariate analysis of factors predictive of long-term survival in patients with HCC

Variable	Hazard ratio (95% CI)	*P* value
Age (years)	1.021 (0.997–1.046)	0.081
Gender (female/male)	0.759 (0.484–1.189)	0.229
HBsAg (negative/positive)	1.401 (0.712–2.759)	0.329
Anti-HCV (negative/positive)	0.916 (0.505–1.663)	0.774
Alcohol intake (not frequent/frequent)	0.740 (0.347–1.601)	0.451
Child–Pugh class (A/B, C)	2.269 (1.509–3.410)	<0.001
Log (AFP ng/ml)	1.310 (1.102–1.558)	0.002
μ-TAS AFP-L3 (<7/≥7)	1.673 (1.079–2.594)	0.021
Log (DCP mAU/ml)	1.220 (0.970–1.534)	0.089
Maximum tumor size (mm)	1.007 (0.994–1.012)	0.511
Tumor number (single/multiple)	2.297 (1.393–3.787)	0.001
Vessel invasion (negative/positive)	2.654 (1.265–5.566)	0.010
Treatment (hepatic resection/RFA, PEI, TACE, and TAI)	1.739 (1.093–2.767)	0.019

HCC hepatocellular carcinoma, *HBsAg* hepatitis B surface antigen, *HCV* hepatitis C virus, *AFP* alpha-fetoprotein, *AFP-L3* fucosylated fraction of AFP, *DCP* des-gamma-carboxy prothrombin, *μ-TAS* micro-total analysis system, *RFA* radiofrequency ablation, *PEI* percutaneous ethanol injection, *TACE* transcatheter arterial chemoembolization, *TAI* transcatheter arterial infusion chemotherapy, *CI* confidence interval. Hazard ratio and *P* values were calculated using Cox's proportional-hazard model

a 7% cutoff value was 2.7-fold (44.2% versus 16.3%) higher than for the LiBASys assay in 43 stage I HCC patients. The detection of early-stage HCC using the μ-TAS assay will increase the opportunity for curative treatment and improve the survival of patients with HCC.

In addition to this high analytical sensitivity, the μ-TAS assay requires only 10 min to determine AFP-L3%, and is a fully automated instrument platform [16]. This shortening of the assay time in comparison with the LiBASys assay, for which the runtime is about 1 h, contributes to its clinical convenience for outpatients with HCC, and will allow clinicians to detect HCC, making it possible to perform prompt imaging diagnosis using modalities such as CT and MRI.

A number of studies have shown that AFP-L3 status is an independent prognostic factor in patients with HCC [9–13]. We previously reported that patients with AFP-L3 positivity of more than 15% had an unfavorable survival rate in comparison with patients showing 15% or less for AFP-L3. Moreover, the differences were more significant in the subgroups with lower AFP concentrations [20]. We demonstrated that μ-TAS AFP-L3 status (<7% or ≥7%) was a factor significantly predictive of long-term survival in patients with HCC, and confirmed that the survival rate of patients with elevated μ-TAS AFP-L3 level (≥7%) was significantly lower than that of patients without such elevation.

In conclusion, the present study has demonstrated that the μ-TAS AFP-L3 value is more sensitive for discriminating HCC than is the conventional LiBASys AFP-L3. This diagnostic sensitivity was especially good in subgroups with lower AFP concentrations, and improved the clinical utility of AFP-L3 for detection of early-stage HCC. In addition, to maximize the utility of this high sensitivity, we suggest that a cutoff value of 7% is most appropriate for discriminating HCC from BLD using this newly developed μ-TAS AFP-L3 assay.

Acknowledgments This study was supported in part by a Grant-in-Aid (20390205), Japan Society for the Promotion Science, and a Grant-in-Aid from Health, Labor, and Welfare, Japan.

References

1. Abelev GI. Production of embryonal serum alpha-globulin by hepatoma: review of experimental and clinical data. *Cancer Res.* 1968;28:1344–1350.
2. Conor GI, Tatarinov YS, Abelev GI, Uriel J. A collaborative study for the evaluation of a serologic test for primary liver cancer. *Cancer.* 1970;25:1091–1098.
3. Bayati N, Silverman AL, Gordon SC. Serum alpha-fetoprotein levels and liver histology in patients with chronic hepatitis C. *Am J Gastroenterol.* 1998;93:2452–2456.
4. Goldstein NS, Blue DE, Hankin R, et al. Serum alpha-fetoprotein levels in patients with chronic hepatitis C. Relationships with serum alanine aminotransferase values, histologic activity index, and hepatocyte MIB-1 scores. *Am J Clin Pathol.* 1999;111:811–816.
5. Chu CW, Hwang SJ, Luo JC, et al. Clinical, virologic, and pathologic significance of elevated serum alpha-fetoprotein levels in patients with chronic hepatitis C. *J Clin Gastroenterol.* 2001;32:240–244.
6. Aoyagi Y, Suzuki Y, Isemura M, et al. The fucosylation index of alpha-fetoprotein and its usefulness in the early diagnosis of hepatocellular carcinoma. *Cancer.* 1988;61:769–774.
7. Aoyagi Y, Saitoh A, Suzuki Y, et al. Fucosylation index of alpha-fetoprotein, a possible aid in the early recognition of hepatocellular carcinoma in patients with cirrhosis. *Hepatology.* 1993;17:50–52.

8. Taketa K, Endo Y, Sekiya C, et al. A collaborative study for the evaluation of lectin-reactive alpha-fetoproteins in early detection of hepatocellular carcinoma. *Cancer Res.* 1993;53:5419–5423.
9. Aoyagi Y, Isokawa O, Suda T, et al. The fucosylation index of alpha-fetoprotein as a possible prognostic indicator for patients with hepatocellular carcinoma. *Cancer.* 1998;83:2076–2082.
10. Hayashi K, Kumada T, Nakano S, et al. Usefulness of measurement of Lens culinaris agglutinin-reactive fraction of alpha-fetoprotein as a marker of prognosis and recurrence of small hepatocellular carcinoma. *Am J Gastroenterol.* 1999;94:3028–3033.
11. Oka H, Saito A, Ito K, et al. Multicenter prospective analysis of newly diagnosed hepatocellular carcinoma with respect to the percentage of Lens culinaris agglutinin-reactive alpha-fetoprotein. *J Gastroenterol Hepatol.* 2001;16:1378–1383.
12. Tateishi R, Shiina S, Yoshida H, et al. Prediction of recurrence of hepatocellular carcinoma after curative ablation using three tumor markers. *Hepatology.* 2006;44:1518–1527.
13. Miyaaki H, Nakashima O, Kurogi M, Eguchi K, Kojiro M. Lens culinaris agglutinin-reactive alpha-fetoprotein and protein induced by vitamin K absence II are potential indicators of a poor prognosis: a histopathological study of surgically resected hepatocellular carcinoma. *J Gastroenterol.* 2007;42:962–968.
14. Nakamura K, Imajo N, Yamagata Y, et al. Liquid-phase binding assay of alpha-fetoprotein using a sulfated antibody for bound/free separation. *Anal Chem.* 1998;70:954–957.
15. Kawabata T, Wada HG, Watanabe M, Satomura S. Electrokinetic analyte transport assay for alpha-fetoprotein immunoassay integrates mixing, reaction and separation on-chip. *Electrophoresis.* 2008;29:1399–1406.
16. Kagebayashi C, Yamaguchi I, Akinaga A, et al. Automated immunoassay system for AFP-L3% using on-chip electrokinetic reaction and separation by affinity electrophoresis. *Anal Biochem.* 2009;388:306–311.
17. Liver Cancer Study Group of Japan. *The general rules for the clinical and pathological study of primary liver cancer, English edn.* Tokyo: Kanehara; 2003.
18. Kudo M, Chung H, Osaki Y. Prognostic staging system for hepatocellular carcinoma (CLIP score): its value and limitations, and a proposal for a new staging system, the Japan Integrated Staging Score (JIS score). *J Gastroenterol.* 2003;38:207–215.
19. Kumada T, Nakano S, Takeda I, et al. Clinical utility of Lens culinaris agglutinin-reactive alpha-fetoprotein in small hepatocellular carcinoma: special reference to imaging diagnosis. *J Hepatol.* 1999;30:125–130.
20. Kobayashi M, Kuroiwa T, Suda T, et al. Fucosylated fraction of alpha-fetoprotein, L3, as a useful prognostic factor in patients with hepatocellular carcinoma with special reference to low concentrations of serum alpha-fetoprotein. *Hepatol Res.* 2007;37:914–922.

Carcinogenesis vol.31 no.3 pp.504–511, 2010
doi:10.1093/carcin/bgp313
Advance Access publication December 16, 2009

IQGAP1 and vimentin are key regulator genes in naturally occurring hepatotumorigenesis induced by oxidative stress

Akihito Tsubota*, Kenji Matsumoto[1], Kaoru Mogushi[2], Koichi Nariai, Yoshihisa Namiki, Sadayori Hoshina, Hiroshi Hano[3], Hiroshi Tanaka[2], Hirohisa Saito[1] and Norio Tada

Institute of Clinical Medicine and Research, Jikei University School of Medicine, 163-1 Kashiwa-shita, Kashiwa, Chiba 277-8567, Japan, [1]Department of Allergy and Immunology, National Research Institute for Child Health and Development, 2-10-1 Okura, Setagaya-ku, Tokyo 157-8535, Japan, [2]Information Center for Medical Sciences, Tokyo Medical and Dental University, 1-5-45 Yushima, Bunkyo-ku, Tokyo 113-8510, Japan and [3]Department of Pathology, Jikei University School of Medicine, 3-25-8 Nishi-Shimbashi, Minato-ku, Tokyo 105-8461, Japan

*To whom correspondence should be addressed. Tel: +81 4 7164 1111 ext. 6601; Fax: +81 4 7166 8638;
Email: atsubo@jikei.ac.jp

To identify key genes involved in the complex multistep process of hepatotumorigenesis, we reduced multivariate clinicopathological variables by using the Long–Evans Cinnamon rat, a model with naturally occurring and oxidative stress-induced hepatotumorigenesis. Gene expression patterns were analyzed serially by profiling liver tissues from rats of a naive status (4 weeks old), through to those with chronic hepatitis (26 and 39 weeks old) to tumor development (67 weeks old). Of 31 099 probe sets used for microarray analysis, 87 were identified as being upregulated in a stepwise manner during disease progression and tumor development. Quantitative real-time reverse transcription–polymerase chain reaction and statistical analyses verified that IQGAP1 and vimentin mRNA expression levels increased significantly throughout hepatotumorigenesis. A hierarchical clustering algorithm showed both genes clustered together and in the same cluster group. Immunohistochemical and western blot analyses showed similar increases in protein levels of IAGAP1 and vimentin. Finally, pathway analyses using text-mining technology with more comprehensive and recent gene–gene interaction data identified IQGAP1 and vimentin as important nodes in underlying gene regulatory networks. These findings enhance our understanding of the multistep hepatotumorigenesis and identification of target molecules for novel treatments.

Introduction

Primary liver cancer ranks third worldwide as a cause for cancer-related mortality, according to World Health Organization reports. The incidence is increasing even in low-endemic Western countries, with hepatocellular carcinoma (HCC) and cholangiocarcinoma accounting for most of these cases. The prognosis for advanced liver cancer remains very poor.

Recent advances in microarray technology have resulted in exponential accumulation of gene expression profiling data and provided novel insights into the molecular mechanisms underlying hepatotumorigenesis (1–3). Nevertheless, the molecular pathogenesis of liver cancer is difficult to establish, because patients present with highly variable clinicopathological features, the risk factors are diverse and liver cancer is heterogenous in nature, both pathologically and biologically (4–7). Such heterogeneity and variation probably underlies the genomic diversity of liver cancer, making it difficult to identify gene signatures in hepatotumorigenesis. In fact, gene expression profiling patterns of HCC differ even between patients with hepatitis B and C virus infections (8,9). Alternatively, it is unclear whether differences in gene expression between tumor and non-tumor tissues represent the cause or consequence of the neoplastic transformation because liver cancer generally evolves through multistep and diverse dysregulated molecular pathways (4).

Liver cancer of any etiology is commonly preceded by chronic inflammation, which is linked tightly to oxidative stress (4,10,11). Indeed, oxidative stress is an important fundamental factor in tumorigenesis that is common to wide-ranging etiologies. For instance, oxidative stress promotes fibrogenesis, serves as an oncogenic mutational mechanism and might accelerate telomere shortening (4,12,13).

Long–Evans Cinnamon (LEC) rats with a genetic deletion in the copper-transporting *Atp7b* gene (14), which is homologous to Wilson's disease gene, exhibit accumulation of large amounts of copper in the liver and spontaneously develop chronic hepatitis, cholangiofibrosis and eventually liver tumor (15–17). Such excessive accumulation of transition metals causes chronic inflammation, characterized by excess production of reactive oxygen species (18), because transition metals interact with physiologically produced reactive oxygen species to catalyze the formation of highly cytotoxic hydroxyl radicals via the Fenton/Haber–Weiss reaction (19). Continuous oxidative stress conditions could be responsible for the pathological processes at play in hepatotumorigenesis (16). Thus, LEC rats could be a useful model to define the multistep mechanisms of hepatotumorigenesis induced by oxidative stress.

To elucidate the molecular mechanisms involved in the multistep hepatotumorigenesis, this study investigated genes that are upregulated in a stepwise manner from the naive liver condition to chronic oxidative stress-induced hepatitis and liver tumor by time-series microarray analysis. The time-dependent gene expression profile should reflect the multistep process of hepatotumorigenesis and identify genes that function specifically in this process. The study also undertook data mining to clarify the impact of candidate genes in the tumor-specific dysregulated gene networks using text-mining technology. These analyses would be helpful not only for a better understanding of the multistep process of liver tumor development but also to identify novel features of known genes and target molecules for treatment.

Materials and methods

Tissue samples

Four-week-old male LEC rats were purchased from Charles River Japan (Yokohama, Japan) and maintained in controlled environments. At 4, 26, 39 and 67 weeks of age, the rats were killed by exsanguination of blood from the abdominal aorta under pentobarbital anesthesia. Paired liver tumor and adjacent non-tumor tissue specimens were obtained from 67-week-old LEC rats (n = 8, Figure 1) that had developed liver tumors. Liver tissues without tumor were obtained from 4-, 26- and 39-week-old LEC rats (n = 6 for each) for analysis of the chronological changes in gene expression profiles. Long–Evans Agouti rats at 67 weeks of age (n = 3), which are wild-type rats, served as the control group (a kind gift from Dr Kozo Matsumoto, Tokushima University, Japan). The Committee for the Care and Use of Laboratory Animals of the Jikei University School of Medicine approved all experimental protocols.

Gene expression analysis

Total RNA was extracted from tissue samples using the RNeasy kit (QIAGEN, Valencia, CA). The RNA integrity was assessed using the Agilent 2100 BioAnalyzer (Agilent Technologies, Palo Alto, CA). A comprehensive gene expression analysis was then performed using 3 μg of total RNA from each sample and the GeneChip® Rat Genome 230 2.0 Array (Affymetrix, Santa Clara, CA) containing 31 099 probe sets, according to the instructions supplied by the manufacturer. To confirm the reproducibility of the results, in the first series of experiments (Figure 1), equivalent amounts of RNA from two pairs randomly selected from eight paired liver tumor and adjacent non-tumor tissue specimens were mixed and analyzed. The average gene expression levels for tumor and non-tumor tissue samples were calculated using the four microarray datasets, respectively. In the following experiments (Figure 1), a mixture of

Abbreviations: HCC, hepatocellular carcinoma; LEC, Long–Evans Cinnamon; RT–PCR, reverse transcription–polymerase chain reaction.

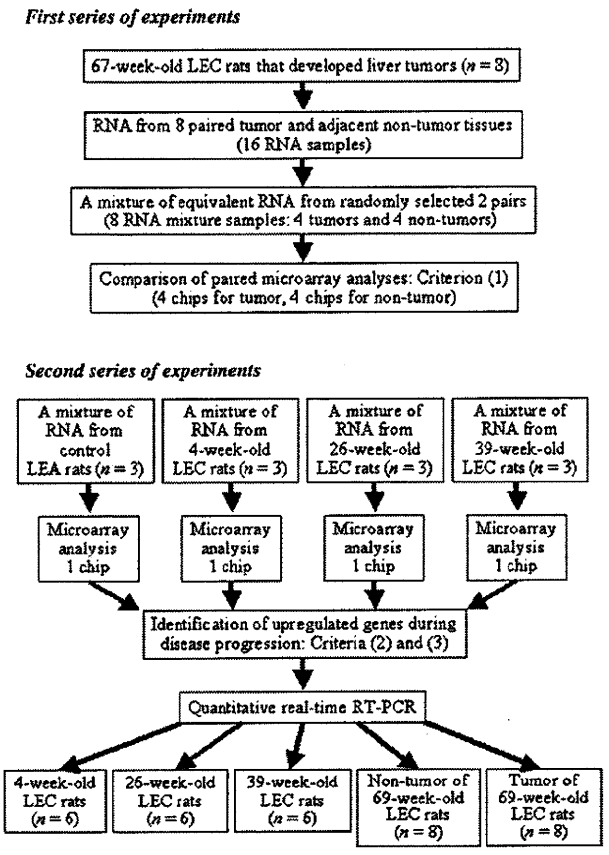

Fig. 1. Analysis flowchart for identification of stepwise upregulated genes during disease progression and multistep hepatotumorigenesis.

equivalent amounts of RNA isolated from LEC rats at 4, 26 and 39 weeks of age and controls (n = 3 for each), respectively, was exploited as an RNA pool for microarray analyses. Microarray datasets were normalized by the robust multi-array analysis, using the R 2.6.1 statistical software together with a BioConductor package (http://www.bioconductor.org/). Normalized expression levels were presented as $\log_2$-transformed values by robust multi-array analysis, and control probe sets were removed for further analysis. To eliminate background signals, genes were selected if their expression was assigned as 'Present' in at least one sample by the GeneChip Operating Software version 1.4 (Affymetrix). A total of 11 305 probes met the quality criteria in the first experiments and were thus subjected to further analysis.

Differential gene expression during disease progression

To identify genes that were upregulated during disease progression and involved in multistep hepatotumorigenesis, each gene was analyzed for fold change and statistical significance using the following three criteria: (i) >2-fold upregulation in tumor tissue samples compared with adjacent non-tumor tissue samples and P values < 0.01 (analyzed by two-tailed, paired t-test); (ii) stepwise increase in relative expression level at weeks 4, 26 and 39, as well as in non-tumor and tumor tissues at week 67 and (iii) relative expression levels at weeks 26 and 39 ('chronic oxidative stress-induced hepatitis phase') and in non-tumor tissue samples higher than the control sample ('no or less oxidative stress status'). The third criterion was important for selection of genes that were considered more strongly influenced by continuous oxidative stress. For paired t-test, false discovery rate was calculated using the Benjamini–Hochberg method. Three similar criteria were applied also to identify downregulated genes: (i) greater than a 2-fold downregulation in tumor tissues compared with adjacent non-tumor tissues and P values < 0.01; (ii) stepwise decrease in relative expression level at weeks 4, 26 and 39, as well as in non-tumor and tumor tissues at week 67 and (iii) relative expression levels at weeks 26 and 39 and in non-tumor tissue samples lower than the control.

Hierarchical clustering

Upregulated and downregulated probe sets were analyzed by hierarchical clustering using the R 2.6.1 statistical software. The gene expression intensities were transformed into Z scores to set the mean expression intensity to 0 and variance to 1 for all genes. Pearson's correlation coefficient was used to calculate a similarity matrix among probe sets. The complete linkage method was used for agglomeration.

Quantitative real-time reverse transcription–polymerase chain reaction

To validate microarray results and to confirm quantitatively any observed differences in gene expression level, each sample was also subjected to reverse transcription–polymerase chain reaction (RT–PCR) and quantitative real-time RT–PCR at least three times using an ABI PRISM 7700 Sequence Detection System (Applied Biosystems, Foster City, CA). Aliquots of RNA were mixed with oligo(dT) primer to obtain complementary DNA using reverse transcriptase. Target genes in the complementary DNA solution were amplified in a PCR mixture containing TaqMan Universal PCR Master Mix (Applied Biosystems), forward and reverse primers and TaqMan probes (Roche Diagnostics, Indianapolis, IN) designed by the Universal Probe Library Assay Design Center (http://www.roche-applied-science.com/sis/rtpcr/upl/adc.jsp). The expression levels of the 18S rat housekeeping gene were also quantified in all samples using the standard primers and TaqMan probe (Applied Biosystems). Differences in gene expression levels among week 4, 26 and 39 samples (n = 6 for each, Figure 1), as well as non-tumor and tumor tissues (n = 8 for both), were examined by one-way analysis of variance followed by Tukey test or Games–Howell procedure, as appropriate. Each dataset was evaluated for normality of distribution by the Shapiro–Wilk test. P values < 0.05 were considered significant. Statistical analyses were performed using the SPSS 17.0 statistical package (SPSS, Chicago, IL).

Immunohistochemistry

Formalin-fixed paraffin-embedded tissue sections were subjected to the streptavidin–biotin–peroxidase complex assay (i-VIEW DAB kit; Ventana Japan, Yokohama, Japan) on the Ventana auto-immunostaining system (Ventana Japan). Slides were pretreated by the recommended procedures for antigen retrieval. The sections were then incubated with rabbit polyclonal and monoclonal antibodies to IQGAP1 (H-109; Santa Cruz Biotechnology, Santa Cruz, CA) and vimentin (Epitomics, Burlingame, CA) at dilutions of 1:500 and 1:200, respectively, for 30 min at room temperature and then washed three times in phosphate-buffered saline. Sections were incubated with the appropriate secondary antibody for 30 min at room temperature.

Western blotting

Liver tissues were homogenized by sonication in lysis buffer. The protein concentration of each tissue lysate was determined using a bicinchoninic acid protein assay kit (Pierce, Rockford, IL). Samples were subjected to sodium dodecyl sulfate–polyacrylamide gel electrophoresis and then electrotransferred onto nitrocellulose membrane. Membranes were blocked with 5% non-fat milk and then probed with the above-described primary antibodies and another for β-actin (Abcam, San Diego, CA). The bound antibodies were visualized with horseradish peroxidase-conjugated secondary antibodies using Enhanced Chemiluminescence western blotting detection reagents (Amersham Pharmacia Biotech, Piscataway, NJ). The substrate reaction was recorded on X-ray film.

Bioinformatics

Pathway analysis was used to clarify the significance of candidate genes in the gene regulatory networks, using GENPAC® (NalaPro Technologies, Tokyo, Japan) and Cytoscape (http://www.cytoscape.org). GENPAC is a novel information extraction system and database for life science using natural language processing/text-mining technology, thereby deducing gene–gene interaction datasets (20). Cytoscape is a visualization and analysis tool for biological pathways (21). Gene ontology annotation was realized by using the GeneCodis 2.0 web tool (http://genecodis.dacya.ucm.es).

Expression of candidate genes in human microarray databases

To determine the expression levels of candidate genes in human liver cancer, we explored and analyzed publicly available microarray datasets of human liver cancer from the National Center for Biotechnology Information Gene Expression Omnibus (GEO: http://www.ncbi.nlm.nih.gov/geo/). For each microarray dataset, differences in the expression levels of candidate genes between human liver cancer and normal liver tissues were examined by Wilcoxon rank-sum test or one-sample t-test, as appropriate.

Results

Stepwise-upregulated genes during the development of liver tumor

Of the 11 305 probe sets filtered, 482 were initially identified as upregulated according to the first criterion of selection. Of these 482 probe sets, 122 met the second criterion. Finally, 87 probe sets (including 22 with no annotation) satisfied the third criterion for

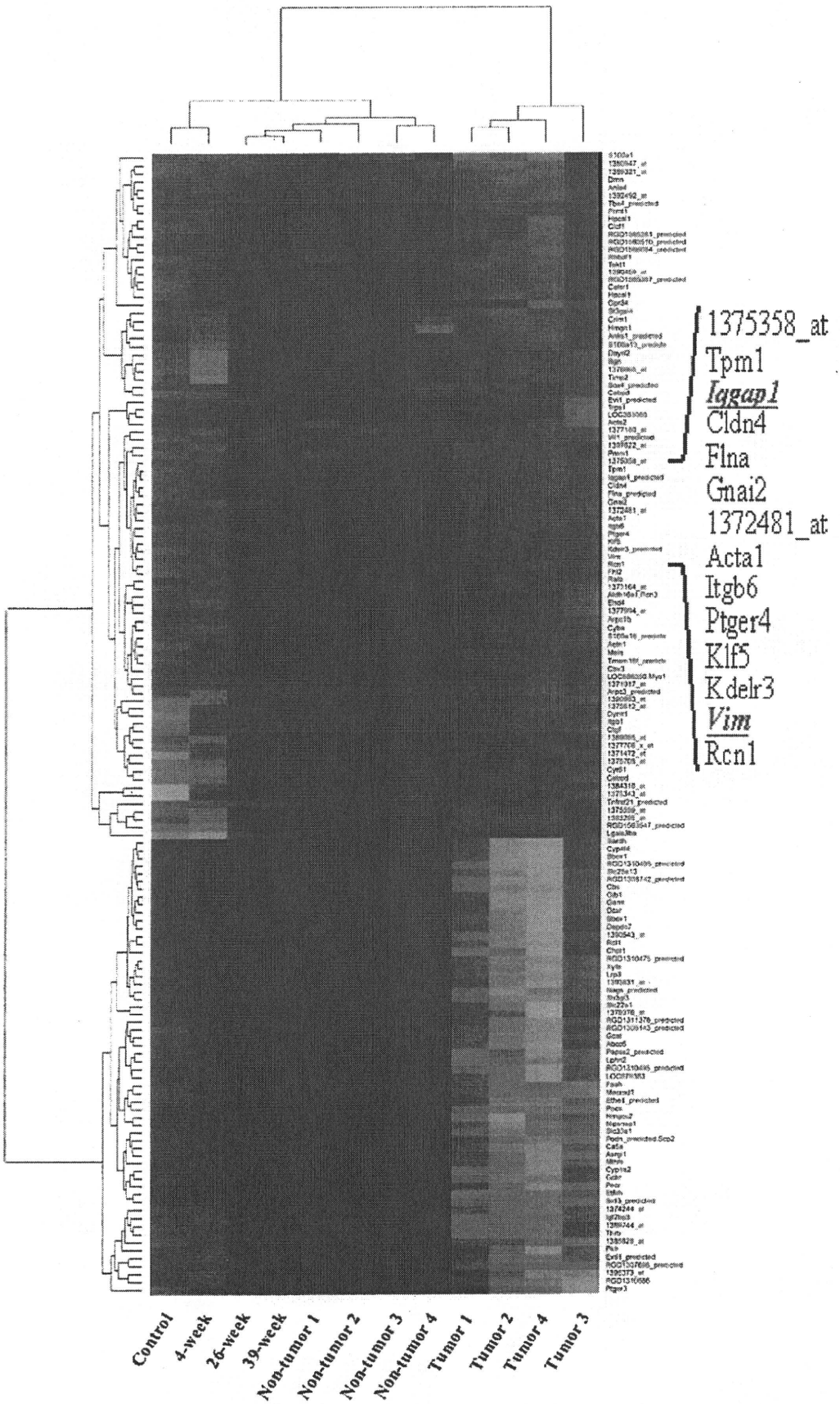
1375358_at
Tpm1
Iqgap1
Cldn4
Flna
Gnai2
1372481_at
Acta1
Itgb6
Ptger4
Klf5
Kdelr3
Vim
Rcn1
Control
4-week
26-week
39-week
Non-tumor 1
Non-tumor 2
Non-tumor 3
Non-tumor 4
Tumor 1
Tumor 2
Tumor 4
Tumor 3

selection (supplementary Table 1 is available at *Carcinogenesis* Online). When the cut-off value for the paired *t*-test for 11 305 probe was set at $P < 0.01$, the estimated false discovery rate was 0.0273. The list contained genes associated with a variety of biological processes, such as cell/cell-matrix adhesion, signal transduction, positive regulation of cell proliferation, integrin-mediated signaling, angiogenesis, regulation of cell growth, positive regulation of the mitogen-activated protein (MAP) kinase kinase kinase cascade, cell motion and inflammatory response. All microarray data have been submitted to Gene Expression Omnibus as GSE17384 ('Gene expression data from the LEC rat model with naturally occurring and oxidative stress-induced liver tumorigenesis'; http://www.ncbi.nlm.nih.gov/geo/). The accession numbers for 'Non-tumor liver at 67 weeks_1 to _4', 'Control liver at 67 weeks', 'Liver at 4, 26 and 39 weeks' and 'Tumor liver at 67 weeks_1 to _4' are GSM434390-3, GSM434394, GSM434395-7 and GSM434398-401, respectively.

Stepwise downregulated genes during the development of liver tumor

Similarly, 58 probe sets (including 7 with no annotation) were identified as being stepwise downregulated during disease progression and tumorigenesis according to all selection criteria (supplementary Table 2 is available at *Carcinogenesis* Online). The list also included genes associated with a variety of molecular functions such as metal/iron ion binding, transferase activity, oxidoreductase activity, protein homodimerization and electron carrier activity.

Two-dimensional hierarchical clustering algorithm

Figure 2 represents the result of hierarchical clustering of the 87 upregulated and 58 downregulated probe sets. A two-dimensional hierarchical clustering algorithm completely distinguished between tumor and non-tumor tissues (Figure 2). The dendrogram shows that samples from 4-week-old LEC and control rats clustered together and formed a statistically different group from samples of 26-, 39- and 67-week-old rats (non-tumor and tumor), indicating that the listed genes were altered by persistent exposure to oxidative stress.

Validation of microarray data by quantitative real-time RT–PCR

To verify the reliability of the microarray data, all the 87 upregulated genes and all time-point samples of each gene were subjected to quantitative real-time RT–PCR. The average mRNA expression levels simply increased in a phased manner in only five genes: connective tissue growth factor (*CTGF*), IQ motif containing GTPase-activating protein 1 (*IQGAP1*), vimentin (*Vim*), smooth muscle alpha-actin (*Acta2*) and reticulocalbin 3 (*Rcn3*). The remaining 82 genes did not show a stepwise increase. Analysis of variance showed significant differences in expression of CTGF, IQGAP1 and vimentin. Finally, *post hoc* analyses showed significant increases in IQGAP1 and vimentin in a stepwise manner during liver disease progression and tumorigenesis (Figure 3). IQGAP1 mRNA levels (mean ± SD) were 0.17 ± 0.15, 0.76 ± 0.21, 1.43 ± 0.49, 2.74 ± 0.34 and 54.33 ± 12.60 in non-tumor liver tissue at week 4, 26, 39 and 67 and tumor tissues, respectively. Similarly, vimentin mRNA levels were 0.0011 ± 0.00035, 0.32 ± 0.08, 0.62 ± 0.28, 4.27 ± 1.92 and 40.78 ± 12.01. All comparisons between two time points except 26 week versus 39 week showed significantly different relative expression levels in both IQGAP1 and vimentin. IQGAP1 and vimentin clustered together and were in the same cluster group (Figure 2).

Immunohistochemical staining and western blot analysis

Next, the expressions of IQGAP1 and vimentin were assessed at the protein level during hepatotumorigenesis by immunohistochemical staining with antibodies against the two proteins (Figure 4A and B). Immunostaining for IQGAP1 and vimentin in the cell membrane or

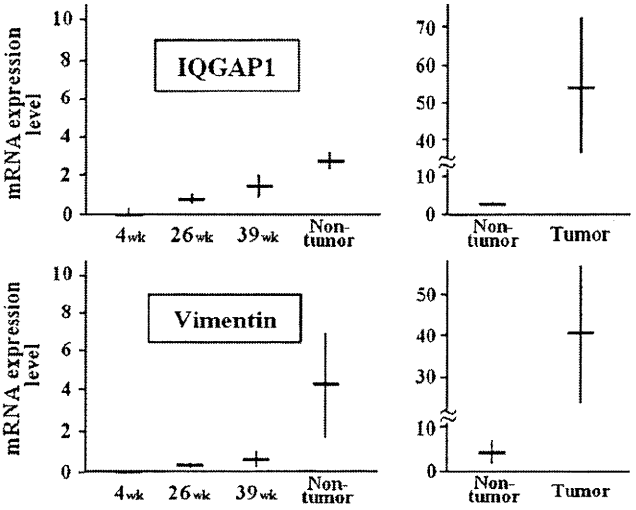

Fig. 3. Validation of differentially expressed genes using quantitative real-time RT–PCR analysis for IQGAP1 and vimentin. One-way analysis of variance and subsequent *post hoc* analyses showed that the expression levels of only two genes, IQGAP1 and vimentin, increased significantly in a stepwise manner during liver disease progression and tumorigenesis. All comparisons between two time points except 26 weeks versus 39 weeks were significantly different in relative expression levels of both IQGAP1 and vimentin ($P < 0.05$).

pericytoplasm gradually increased with time. The cytoplasm of hepatocytes and lymphocytes showed IQGAP1 staining and strongly immunopositive cells were observed in tumor tissues. Western blotting confirmed the immunostaining results for IQGAP1 and vimentin according to the stepwise progression of hepatocarcinogenesis (Figure 4C).

IQGAP1 and vimentin interact with other genes in gene regulatory networks

To provide insights into the relationship of *IQGAP1* and *vimentin* in underlying gene regulatory networks, microarray data and array-independent text mining were integrated by using GENEPAC and Cytoscape. Sixty-five upregulated known functional genes were related to another 470 genes and connected by 1009 interaction edges (supplementary Figure 1 is available at *Carcinogenesis* Online). *IQGAP1* and *vimentin* were identified as important nodes in the network graph and considered as key regulators. Figure 5A extracted from the interactive graph illustrates the direct relationship of *IQGAP1* and *vimentin* with 37 and 18 other regulatory genes, respectively, including *CDH1* (*E-cadherin*) connecting *IQGAP1* and *vimentin*.

We then explored the relationship of these genes to 'oxidative stress'-related, 'carcinogenesis/tumorigenesis'-related or 'fibrogenesis'-related genes. The number of genes that were related to each category and the degree of overlap between gene sets are shown in Figure 5B. Among 38 genes connected directly with *IQGAP1*, 31 and 31 were related to 'oxidative stress' and 'carcinogenesis/tumorigenesis', respectively. Twenty and 8 of 38 genes were associated with both and all categories, respectively. Among 19 genes connected directly with *vimentin*, 15 were related to 'oxidative stress' and 'carcinogenesis/tumorigenesis'. Five of 19 genes were associated with all categories.

IQGAP1 and vimentin in human liver cancer

IQGAP1 and vimentin were significantly upregulated in microarray datasets of human liver cancer (GSE 4108 and GSE14323). In the

Fig. 2. A two-dimensional hierarchical clustering algorithm of gene expression using probe sets for 87 upregulated and 58 downregulated genes. The horizontal and vertical axes of the dendrogram indicate the degree of similarity between genes and liver tissue samples, respectively, as determined by hierarchical clustering. The gene expression changes are presented in graduated color patches from green (least expression) to red (most abundant expression). IQGAP1 and vimentin were classified into the same cluster group. The vertical dendrogram reflects the clinical course during liver disease progression and tumorigenesis.

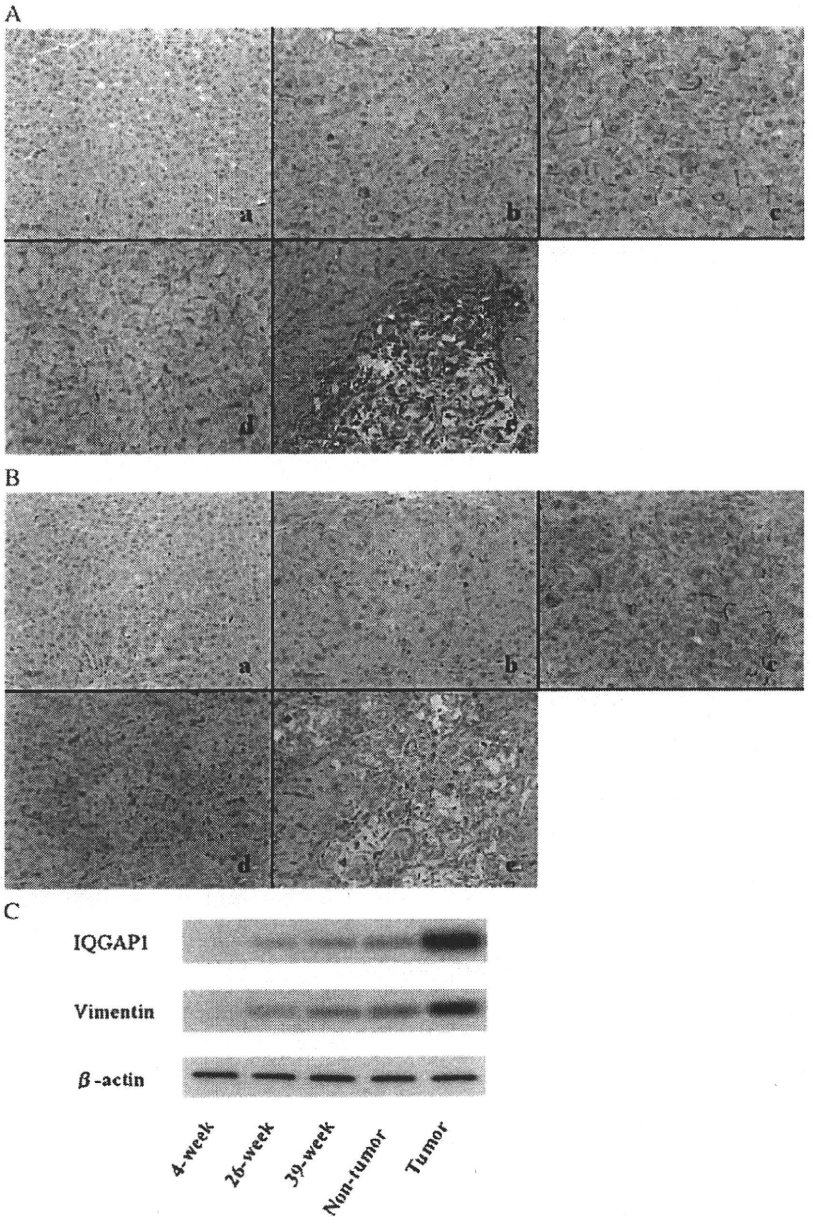

Fig. 4. Immunohistochemical reactivity and western blot analysis of IQGAP1 and vimentin in liver tissue from 4-, 26- and 39-week-old LEC rats (a, b and c), as well as in non-tumor (d) and tumor tissue (e) from 67-week-old LEC rats. (**A**) IQGAP1 staining was prominent at the cell–cell boundaries and cytoplasm according to the stepwise progression of hepatocarcinogenesis. (**B**) Vimentin staining was prominent at the cell–cell boundaries and cytoplasm according to the stepwise progression of hepatocarcinogenesis; bar = 50 μm. (**C**) Western blot analyses. β-Actin was also blotted, as a control. Results are representative data of at least three separate experiments.

GSE4108, the two genes were significantly upregulated in HCC, compared with normal liver tissue ($P = 1.76 \times 10^{-2}$ and 1.69×10^{-6}, respectively; supplementary Figure 2A is available at *Carcinogenesis* Online). In the GSE14323, the two genes were also significantly upregulated in HCC ($P = 7.43 \times 10^{-7}/5.02 \times 10^{-9}$ and 5.97×10^{-14}, respectively; supplementary Figure 2B is available at *Carcinogenesis* Online).

Discussion

To identify specific genes involved in multistep tumorigenesis, multivariate clinicopathological variables should be reduced and simple comparisons between tumor and non-tumor tissues should be avoided. Instead, in the present study, an animal model in which liver tumor developed naturally due to oxidative stress was prepared for microarray analysis to analyze serial changes in gene expression profiles from naive liver status to chronic hepatitis to tumor development. Such conditions or examinations cannot be reproduced or performed in human subjects. The analyses identified IQGAP1 and vimentin as stepwise-upregulated genes throughout the oxidative stress-induced process of hepatotumorigenesis, implicating both as reactive to persistent oxidative stress and important molecules in the mechanism of hepatotumorigenesis. In fact, the GEO database shows that IQGAP1 and vimentin are significantly upregulated in human HCC tissues (GSE4108 and

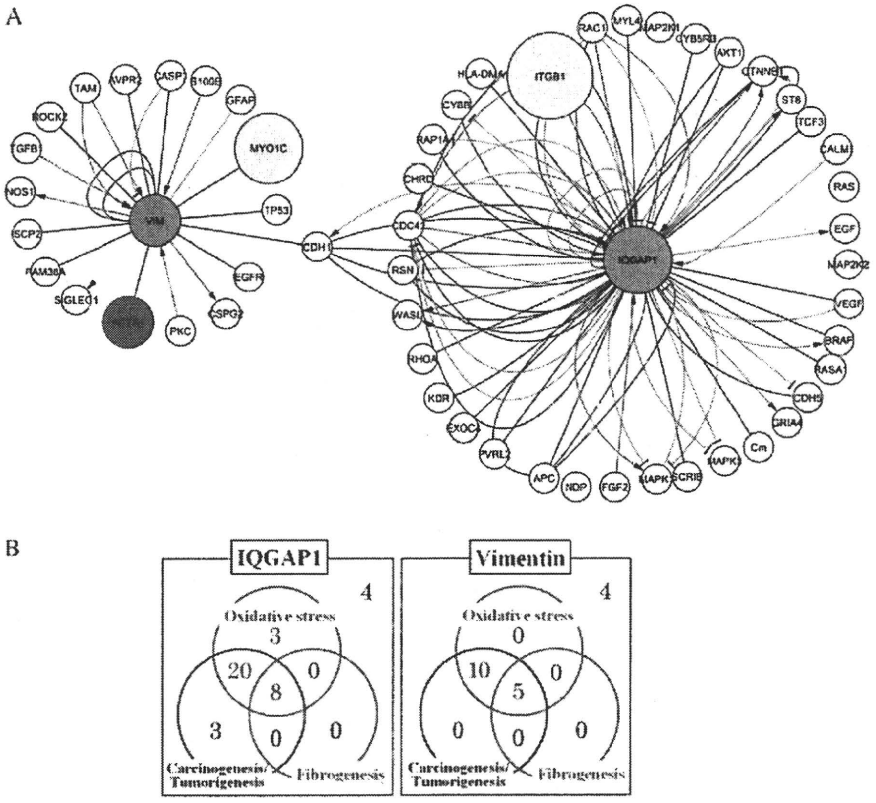

Fig. 5. *IQGAP1*, *vimentin* and related genes. (**A**) Part of the gene regulatory networks for *IQGAP1* and *vimentin*. Microarray data and array-independent text mining were integrated by gene regulatory network analysis (GENPAC). The interaction data were visualized and analyzed by Cytoscape. *CDH1* (*E-cadherin*) is directly linked to both *IQGAP1* and *vimentin*. Color nodes indicate relative overexpression of genes (fold change of tumor to non-tumor) on the microarray data: violet, 4> to ≥2; pale red, 16> to ≥4; red, ≥16 and white, 2> or no data. Node size indicates the proportion of the downstream effectors to the upstream modulators, of which genes are components of various signaling pathways. Edge colors and shapes reflect the interactions between genes: blue, upregulation type, such as 'activate'; red, downregulation type, such as 'inhibit'; green, regulation type, such as 'modulate' without information of up/downregulation; yellow, biochemical type, such as 'phosphorylation' and black, other types, such as 'associate'. (**B**) Biological backgrounds of genes linked directly to *IQGAP1* and *vimentin*. Among 38 genes linked directly to *IQGAP1*, 31 and 31 were related to 'oxidative stress' and 'carcinogenesis/tumorigenesis', respectively. Twenty and 8 of 38 genes were associated with both and all key words, respectively. Among 19 genes connected directly with *vimentin*, 15 were related to 'oxidative stress' and 'carcinogenesis/tumorigenesis'. Five of 19 genes were associated with all categories.

GSE14323, supplementary Figure 2 is available at *Carcinogenesis* Online), relative to other normal liver tissues. This was also confirmed in 165 of our patients with HCC ($P = 1.40 \times 10^{-4}$ and 4.97×10^{-3}, respectively; M.Kaoru and T.Hiroshi, unpublished data).

IQGAP1 is a scaffolding protein that specifically interacts with diverse proteins via multiple motifs. By doing so, IQGAP1 mediates multiprotein complex assembly and regulates multiple physiological cellular processes, such as cell–cell adhesion, cell polarization, cell migration, transcription and regulation of actin cytoskeleton formation and MAP kinase (MAPK) signaling. In addition, many IQGAP1-binding partners are implicated in tumorigenesis and/or tumor progression, including Rac1, Cdc42, Rap1, E-cadherin, β-catenin, components of the MAPK pathway, calmodulin, actin and APC (22–25). IQGAP1 is a downstream effector of Cdc42 and Rac1 (members of the Rho GTPase family). It localizes and interacts with the cytoplasmic domain of E-cadherin (CDH1), β-catenin (CTNNB1) and α-catenin at the cytoplasmic side of adherens junctions to negatively regulate E-cadherin-mediated cell–cell adhesion by interacting with β-catenin and dissociating α-catenin from the cadherin–catenin complex. Activated Cdc42 and Rac1 inhibit IQGAP1, thereby stabilizing the E-cadherin complex link to actin cytoskeleton and ensuring strong and rigid adhesion. Conversely, non-suppressed IQGAP1 results in diminished cell–cell adhesion (22,25,26). In human breast epithelial cells, IQGAP1 contributes to neoplastic transformation, upregulation of cell proliferation, angiogenesis, invasion and high metastatic capacity *in vitro*. Conversely, knockdown of IQGAP1 substantially reduces the amount of active Cdc42 and Rac1 in breast carcinoma *in vivo*. Cdc42/Rac1 and actin participate in IQGAP1-stimulated tumorigenesis, invasion and proliferation (27). In human gastric cancer, the expression levels of Rac1 and IQGAP1 are significantly correlated, while tumors showing E-cadherin mutations have reduced or absent levels of both (28). IQGAP1 also directly interacts with vascular endothelial growth factor type-2 receptor, via which reactive oxygen species derived from Rac1-dependent NAD(P)H oxidase are involved in vascular endothelial growth factor signaling, thereby promoting endothelial cell migration and proliferation that are important for angiogenesis (29). IQGAP1 activates B-Raf to mediate endothelial cell proliferation, which is essential for vascular endothelial growth factor to stimulate angiogenesis (30).

The IQGAP1 gene and/or protein is overexpressed in several human neoplasms: gastric (28,31,32), lung (33), colorectal (34), ovarian (35) and glioblastoma (36). From a clinical aspect, IQGAP1 seems closely associated with tumor invasion and metastasis and with the progression and poor prognosis of malignancies. However, it is not known whether IQGAP1 is the cause or consequence of neoplastic transformation. The present study analyzed the average levels of IQGAP1 mRNA and found increases of >4-fold, >8-fold and >16-fold in non-tumor liver tissues of rats at weeks 26, 39 and 67, respectively, compared with 4-week-old animals (Figure 3). This indicated that IQGAP1 expression was latently upregulated before development of the liver tumor. The immunohistochemical and western blotting results (Figure 4)